THE JOURNAL OF PHYSICAL CHEMISTRY C
A JOURNAL OF THE AMERICAN CHEMICAL SOCIETY

pubs.acs.org/JPCC

Perspective

Plasmonic Nanobubbles—A Perspective

Seunghyun Moon, Qiushi Zhang, Zhihao Xu, Dezhao Huang, Seongmin Kim, Jarrod Schiffbauer,* Eungkyu Lee,* and Tengfei Luo*

Cite This: https://doi.org/10.1021/acs.jpcc.1c07244

Read Online

ACCESS | Metrics & More | Article Recommendations

ABSTRACT: The field of plasmonic nanobubbles, referring to bubbles generated around nanoparticles due to plasmonic heating, is growing rapidly in recent years. Theoretical, simulation, and experimental studies have been reported to reveal the fundamental physics related to this nanoscale multiphysics phenomenon. Using plasmonic nanobubbles for applications is in the early stage but progressing. In this Perspective, we briefly review the current state of this research field and give our perspectives on the research needs in the theoretical, simulation, and experimental fronts. We also give our perspectives on how the fundamental understanding can be applied to more practical applications.

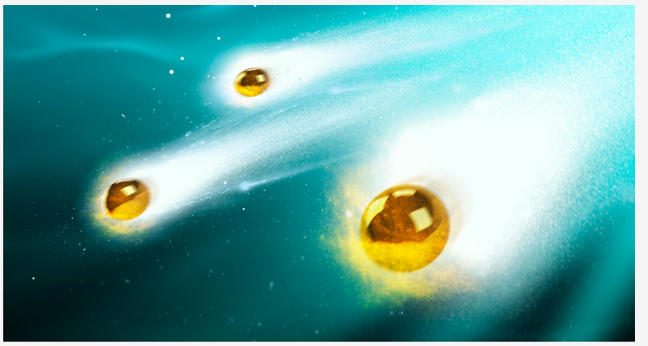

1. INTRODUCTION

Because of surface plasmon resonance (SPR), plasmonic nanoparticles (NPs) can efficiently convert photon energy into heat when excited by light at the SPR frequency. Such intensely heated NPs can locally generate the so-called plasmonic nanobubbles. Such nanobubbles can be made of vapor, dissolved gas, or their combinations, and they usually have diameters on the order of several tens to hundreds of nanometers. These nanobubbles are known for their unique photothermal and optical properties and have already led to biomedical applications in cell-level therapy and imaging, controlled drug release and delivery, microtissue surgery, and biosensing, with some already entered into clinical trials.[1−5] They are also studied for energy and fluidic applications like solar-vapor generation,[6,7] plasmon-assisted photocatalytic reactions,[8] optofluidics,[9] nano swimmers,[10] surface bubble manipulation,[11] and materials assembly.[12] In case the plasmonic NPs are immobilized or fabricated on a substrate, they can form bubbles on the surface upon optical excitation, and we refer to them as plasmonic surface bubbles, but our focus in this article is on plasmonic nanobubbles, which are formed around NPs suspended in liquids.

Besides the promises in applications, the fundamentals of plasmonic nanobubbles are no less attractive. The physics involved in this molecular- to nanometer-scale phenomenon is complicated, and studies have tried to understand it from different angles. The respective roles of surface chemistry, curvature, viscosity, and surface tension in bubble formation and subsequent dynamics have been at the focus of theoretical and numerical investigations of plasmonic nanobubbles for over a decade,[13−17] but they are not fully resolved. The inherently multiscale thermodynamics of phase change at nanoscale-curved solid−fluid interfaces poses several challenges from a theoretical viewpoint. The $1/r$ (where r is the radius of an NP) interfacial contributions to the free energy, surface−solvent interactions, solvent properties, and competition between time scales of NP heating and cooling all play important roles in the nucleation and subsequent dynamics of a plasmonic nanobubble, leading to effects such as an experimentally observed minimum in the threshold fluence,[14,16] explosive bubble collapse and oscillations,[18,19] and reported NP surface temperatures above the melting point of gold.[18,20,26,76] Several theoretical approaches have been brought to bear on these problems,[19,21−24] elucidating the underlying complexities of the problem in doing so, especially for bubble nucleation and dynamics for NPs with radii of tens of nanometers and smaller. However, in general, these theoretical approaches have relied on simplified fluid models for a single species of the molecule, while the complexities of experimentally relevant multicomponent fluids are often ignored.

In this Perspective, we briefly review the current state of the field of plasmonic nanobubbles, but instead of a comprehensive review, we focus on what we believe to be fundamentally interesting and give our perspectives on the challenges and

Received: August 16, 2021
Revised: September 30, 2021

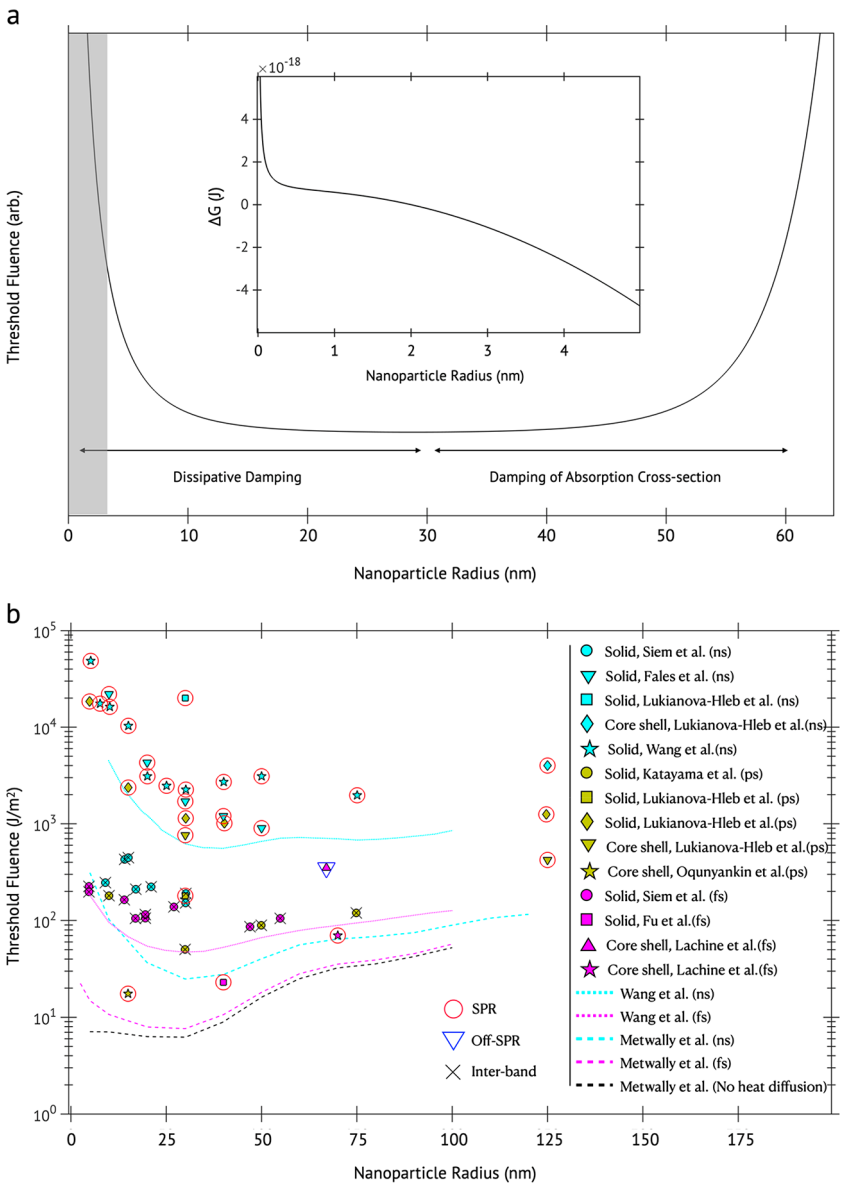

Figure 1. (a) Schematic of threshold fluence vs NP radius for general pulsed heating cases showing the ubiquitous bathtub minimum determined by the competition between heating and cooling time scales. At a sufficiently small radius (gray shaded region), the formation of vapor becomes interface-controlled, and the detailed properties of the fluid and the wetting properties of the interface must be considered along with the thermodynamics of the NP itself. This is explained by the inset showing the Gibbs energy change for nucleation of an ∼1 nm thick vapor layer around a moderately hydrophilic NP from liquid argon in thermal equilibrium at the liquid argon spinodal. For NPs smaller than 2 nm in this fluid, no stable bubble can be formed, in agreement with the nonequilibrium MD results of Sasikumar et al.[22] (b) Nanobubble formation fluence threshold as a function of radius of Au NP for different laser pulse durations. Legends describe the type of NP, reference, and laser pulse duration in parentheses: Solid, Siem et al. (ns);[14] Solid, Fales et al. (ns);[27] Solid, Lukianova-Hleb et al. (ns);[16] Core−Shell, Lukianova-Hleb et al. (ns);[13] Solid, Wang et al. (ns);[26] Solid, Katayama et al. (ps);[15] Solid, (square) Lukianova-Hleb et al. (ps);[16] Solid, (diamond) Lukianova-Hleb et al. (ps);[13] Core−Shell, Lukianova-Hleb et al. (ps);[13] Core−Shell, Oqunyankin et al. (ps);[28] Solid, Siem et al. (fs);[14] Solid, Fu et al. (fs);[29] Core−Shell, Lachaine et al. (fs);[30] (dotted lines) Wang et al.;[26] (dash lines) Metwally et al.[23]

unresolved questions in the theoretical, simulation, and experimental fronts. We will emphasize the fundamentals of plasmonic nanobubbles but will also touch on their application aspects. Besides, we also briefly discuss plasmonic surface bubbles when they are related to plasmonic nanobubbles.

2. DISCUSSION AND PERSPECTIVE

Two of the main questions that have driven much of the fundamental research on plasmonic nanobubbles are (1) how are nanobubbles generated upon optical excitation? and (2) what are the bubble dynamics? Answering these questions is no easy task. On the one hand, the nanometer bubble size and generally subnano-to-picosecond dynamics makes the experimental study of nanobubbles challenging, while on the other hand, the complex interplay of fluid transport properties and surface forces in confined or highly curved geometries makes unraveling the mechanisms underlying these issues a difficult task from a theoretical perspective. In the following sections, we will discuss the state of addressing each of these questions.

2.1. Plasmonic Nanobubble Formation. Theoretically, much of the focus has been on the role of NP diameter, laser pulse duration (τ), and Kapitza resistance (i.e., interfacial

https://doi.org/10.1021/acs.jpcc.1c07244
J. Phys. Chem. C XXXX, XXX, XXX−XXX

thermal resistance between NP and solvent)[23] on the fluence threshold for plasmonic nanobubble formation. However, the dissipative properties of the fluid and thermodynamics of the NP are also found as critical in determining the heat flux from the hot particle to the surrounding fluid.[24,25] Metwally et al.[23] demonstrated that, for a pulsed heating of NPs in a simple, uniform solvent, the origins of the minimum in the fluence threshold for NPs with a radius r of ∼20−30 nm lie chiefly in a competition between the time scales of the electron−photon interaction and that of diffusive cooling. At NP radii below this, diffusive losses to the environment require an increasingly higher fluence for the NP surface to reach the spinodal temperature of the solvent, with larger losses at longer pulse durations. With increases in the radius much above 20−30 nm, a damping of the absorption cross-section results in a deviation from its linear dependence on the NP volume, leading to an increase in the fluence threshold (Figure 1a). For sufficiently large NPs, the diffusive cooling time will generally be larger than the thermal relaxation time associated with the interfacial thermal conductance; thus, Metwally et al.[23] conclude that interfacial thermal conductance plays a negligible role in the determination of threshold fluence. However, because the variation of thermal properties and phase of the surrounding fluid are not accounted for, the applicability their conclusions regarding the role of interfacial thermal conductance may be restricted to nanostructures with sufficiently large radii of curvature, that is, accordingly for $r \gg \kappa/G$, where κ is the solvent thermal conductivity, and G is the interfacial thermal conductance. Thus, as a practical example, for gold−water interfaces, this implies that NPs with radii of curvature much smaller than ∼4 nm require further consideration (shaded area in Figure 1a), but such small NPs are not often seen in applications. However, as shown by Wang et al.,[26] accounting for the full thermodynamics of the NP, interfacial thermal conductance, pulse duration, and wavelength (λ) can become critical factors, shifting the overall threshold fluence curve upward around the 20−80 nm range (in water) and yielding criteria for optimally "biosafe" NP bubble nucleation. At radii much below or above this level, the competition between dissipation and absorption overshadows the role of a structural/phase change in the NP.

Overall, the competition between heating and cooling time scales for NPs with different sizes would lead to a ubiquitous "bathtub" minimum in the fluence threshold for nanobubble formation (Figure 1a). This trend can generally explain experimental observations from different studies. Figure 1b summarizes the fluence thresholds for plasmonic nanobubble formation around Au NPs with various sizes reported in the past decade. Most of the experiments have used solid spherical Au NPs immersed in water, since these NPs can be easily synthesized and tuned in size. In Figure 1b, we can have the following key observations that shed light on different influential thermal and optical behaviors of the system of interest.

First, smaller Au NPs usually have higher fluence thresholds in each experimental setup. As the NP size gets smaller, it has a smaller thermal mass and larger surface-to-volume ratio, which renders more efficient heat dissipation to the solvent and faster cooling of the NP. A higher fluence is then required to balance the faster cooling to reach the bubble formation threshold. The predictions by the models from Metwally et al. (dash lines)[23] and Wang et al. (dotted lines)[26] clearly show such threshold increments for small NPs very well. Without a consideration of the enhanced heat diffusion for such NPs, Metwally's model would show that the increased fluence threshold no longer exists (black dash line). At the other extreme, when the NP size gets large, its thermal mass increases, and the optical absorption per volume usually decreases. Thus, the fluence threshold will also increase, which can also be predicted correctly by the models. The crossover of these two opposite trends leads to the ubiquitous bathtub with a minimum in the fluence threshold as a function of the NP size.

Second, the fluence threshold differs for different excitation laser pulse durations. The fluence influences the total energy that can be deposited in a pulse, and the pulse duration controls the photon−electron energy transfer rate. An interesting observation in Figure 1b is that, for the picosecond or nanosecond pulse durations, the optical excitation at the interband transition frequency (near 330 or 470 nm)[31] enables the bubble generation at a lower fluence than that at the SPR frequency. This is not intuitive because, at the SPR, the free electron gas in the NP strongly interacts with the incident photon, leading to a stronger optical absorption and thus more intense heating than that at the interband transition frequency. As a result, the SPR excitation should have a lower fluence threshold than that of the interband excitation. This is the prediction by Metwally et al.[23] for an SPR excitation (cyan dash line) that is 1 order of magnitude smaller than those of experimental sets with the interband excitation (cyan circle, τ = 10 ns, λ = 355 nm: interband). However, the measured threshold fluences at the SPR excitation differ from the model prediction[23] by 2 orders of magnitude. One possible reason for the difference is that the SPR is sensitive to the change of refractive indices of the system. When the pulse duration is comparable to the electron−phonon relaxation time (1−2 ps),[23] the thermal energy can be released from the hot electrons during the laser absorption process, which increases the temperature of the NP and medium (e.g., water) and thus changes their refractive indices. Indeed, Wang et al.[26] found that the medium (e.g., surrounding water) heating can suppress the SPR effect. This is also known as SPR bleaching, which limits an NP's ability to fully leverage the incident photon in a pulse. When Wang et al.[26] consider the temperature-dependent optical absorption efficiency of NP in their model, the predicted threshold fluence (cyan dotted line, τ = 5 ns, λ = 530 nm: SPR) becomes closer to the experimental result, but they still differ by 1 order of magnitude. On the one hand, the reason for this discrepancy remains an open question to be answered. On the other hand, the interband transition is not sensitive to temperature change, as it is related to the band-to-band transition of an electron by absorbing a photon. As a result, the optical absorption will not be significantly affected in the photothermal heating process, which may have led the interband excitation threshold fluence to be lower than the SPR cases. However, using a femtosecond pulsed laser can avoid the SPR bleaching effect. The characteristic time of medium heating by the cooling of Au NP is ∼100 ps,[32] which is longer than the electron−phonon relaxation time; thus, femtosecond pulses can finish the interaction with electrons before the medium heating. Indeed, Fu et al.[29] used a four-dimensional (4D) transmission electron microscope to visualize the nanobubble generation around solid Au NPs and found that a femtosecond pulse at the SPR with a fluence of 23 J m^{2-} could form a nanobubble on the NP (pink square, τ = 350 fs, λ = 520 nm: SPR). This reported value is close to the predicted threshold fluence by Metwally et al.[23] (pink dash line). Also,

https://doi.org/10.1021/acs.jpcc.1c07244
J. Phys. Chem. C XXXX, XXX, XXX−XXX

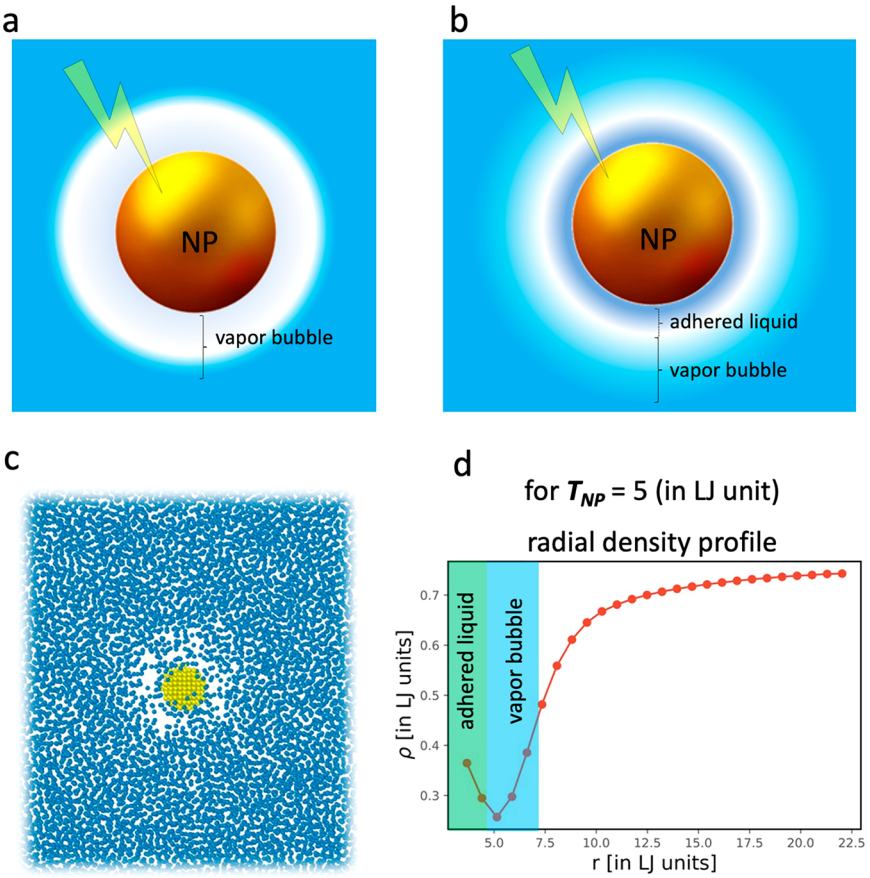

Figure 2. Schematics of (a) a dry bubble and (b) a bubble with an adhered liquid layer on the NP surface. MD simulation snapshot showing an adhered liquid layer (c), which is quantified by the radial density profile (d) for NP heated to T_{NP} = 5 in LJ unit.

Fu's threshold fluence is much smaller than the measured fluence with interband transition excitation with a femtosecond pulse (pink circle and pink dotted line, τ = 100 fs, λ = 400 nm: interband). Therefore, it may be preferential to use a femtosecond pulsed laser to leverage the SPR effect in plasmonic nanobubble applications.

It is worth noting that Metwally et al.[23] emphasize the water spinodal temperature (~550 K) as the correct thermodynamic criterion for liquid–vapor transition, rather than referring to the critical temperature. But in the presence of highly curved surfaces, and accounting for the role of surface forces and wettability on the thermodynamics of phase change at the interface as well as the interfacial thermal conductance,[33,34] the liquid spinodal itself can shift.[35,36] The equilibrium and nonequilibrium thermodynamics of phase change near heated NP interfaces has been studied using both molecular dynamics[21,22] and continuum/phase-field methods.[24] Both liquid–vapor and solid–liquid interfacial energetic costs must be met to create a stable bubble. However, in general, the solid–vapor interfacial energy cost is higher. This is owing both to the larger surface energy per unit area required to create a dry surface, especially for a hydrophilic interface, as well as the fact that the inner NP radius is smaller than the radius at the liquid–vapor interface. Rather than resulting in a dry interface (Figure 2a), for hydrophilic surfaces, this fact leads to the stabilization of a superheated liquid layer adjacent to the NP surface (Figure 2b);[21,22,24] the energetic cost of forming an interface with such a layer will necessarily be lower than that of a dry interface. This phenomenon has been observed in molecular dynamics (MD) simulations,[37] which show a layer of liquid molecules adhered to the NP surface despite a vapor bubble being formed when the NP is sufficiently heated (Figure 2c,d). However, the thermodynamic properties of this thin liquid layer, including its Gibbs energy at equilibrium, are presumably quite distinct from that of the liquid bulk or the usual liquid–vapor interface. While an equilibrium Gibbs energy criterion for a "dry" NP bubble[24] (see Figure 1a inset) can lead to estimates for equilibrium and critical NP radii for a bubble nucleation in good quantitative agreement with simulations of hydrophilic NPs as well as estimates for equilibrium bubble size for a given NP, it is not yet clear that the thermodynamic properties of this liquid layer can be included in such a formulation in a straightforward way. Nonequilibrium continuum thermodynamics can capture the stabilization of the superheated liquid layer.[24]

It is worth noting that, while the photothermal phase change interpretation remains to be the mainstream to understand the plasmonic nanobubble formation, Lachaine et al.[30] proposed a very different mechanism for nanobubble formation. They have shown that, at off-SPR wavelengths, the Au NP can still form a nanobubble but at a lower fluence threshold and corresponding to a quite different, lower-energy near-field photoionization mechanism. It is possible that both mechanisms could be operative under a broad band illumination. Such bubbles could be expected to have quite different bubble dynamics, a point that would require further investigation.

When the fluence threshold is being determined, a prerequisite is the ability to detect the nanobubble formation.

https://doi.org/10.1021/acs.jpcc.1c07244
J. Phys. Chem. C XXXX, XXX, XXX–XXX

Since the formation of nanobubbles can change the scattered light intensity, optical pump−probe transient scattering methods have been used to detect the nanobubble formation. The pump beam is the excitation laser, while the probe beam, much weaker in energy than the pump beam, can be set at the wavelength where the variation of scattering efficiency is sensitive to the nanobubble formation.[10] Since nanobubble formation is accompanied by an acoustic wave, the acoustic response has also been used for this detection.[26,27] A direct observation of nanobubble formation has also become possible when a time-resolved transmission electron microscope is employed.[29]

2.2. Nanobubble Dynamics. The bubble dynamics, lifetime, and eventual collapse involve a more detailed consideration of the properties of the fluid and fluid−vapor interface. Phase-field models and the Rayleigh-Plesset equation have been shown to yield comparable bubble dynamics including collapse and oscillations,[18,38] where the dynamics depend on the heating condition (hence thermodynamics) of the NP.[19] Sasikumar and Keblinski[38] identified four distinct stages of nanobubble formation: (1) nucleation and adiabatic expansion of hot vapor, (2) isothermal expansion, (3) isothermal collapse, and (4) rapid heating. The range of times for bubble dynamics depends somewhat on the NP size as well as the properties and composition of the fluid. However, allowing for these differences, Sasikumar and Keblinski's MD simulations[38] agree well with the experimental observations and continuum simulations of Kotaidis and Plech,[18] with the initial adiabatic expansion occurring during the first ∼50−100 ps, followed by an expansion and collapse over the next 100 ps to 1 ns.

Recent experimental studies[39,40] demonstrate that physicochemical factors such as dissolved gas or other solutes, especially as they modify the surface tension and viscosity, are important, particularly in the dynamics of bubble collapse. However, in these studies, it is not clear how the thermodynamic and physicochemical properties of the solvent itself, independent from the changes in effective thermophysical properties due to the NPs themselves, affect bubble dynamics. One often ignored consideration in modeling and theory is the role of dissolved gas at the liquid−vapor interface, which has been recently shown[40] to have a profound effect on bubble collapse dynamics. In addition to contributions to the bulk solvent properties, dissolved gases can severely impact the structure and composition of liquid−vapor and fluid−solid interfaces and, thereby, play an important role in both nanobubble nucleation and collapse dynamics. Overall, the issue of the role of dissolved gases on the interfacial behavior in fluids is complex and not well-understood. Through both ionic and nonionic mechanisms, ranging from simple steric contributions to the interfacial structure to possible induced dipole or even Casimir effects,[41] dissolved gases can dramatically alter the balance and nature of interfacial forces governing capillary phenomena. Thus, an important direction for further work in plasmonic-generated bubbles can include detailed studies of the nonequilibrium thermodynamics of multicomponent solutions and the role of high curvature/specific area.

2.3. NP Dynamics with Nanobubbles. Beyond bubble nucleation and subsequent dynamics, another issue of importance is the possible motion of an NP within a nanobubble. Here, it is worth noting that, while the problem can be treated in the framework of a driven Brownian motion, the near-particle gradients in temperature, density, and viscosity can lead to complexities in the determination of the effective friction,[42] and such effects become more localized and dominate the NP dynamics when a nanobubble is formed to encapsulate it (i.e., supercavitating NP). Huang et al.[37] used MD simulations to resolve the nonequilibrium multiphase phenomena of a moving supercavitating NP. MD simulations can directly capture the distributions of water molecules around the hot NP without assuming the phase domain. They found that an intensely heated supercavitating NP would exhibit a ballistic Brownian motion with the effective friction similar to that in a gas (Figure 3a). The key is that the NP is

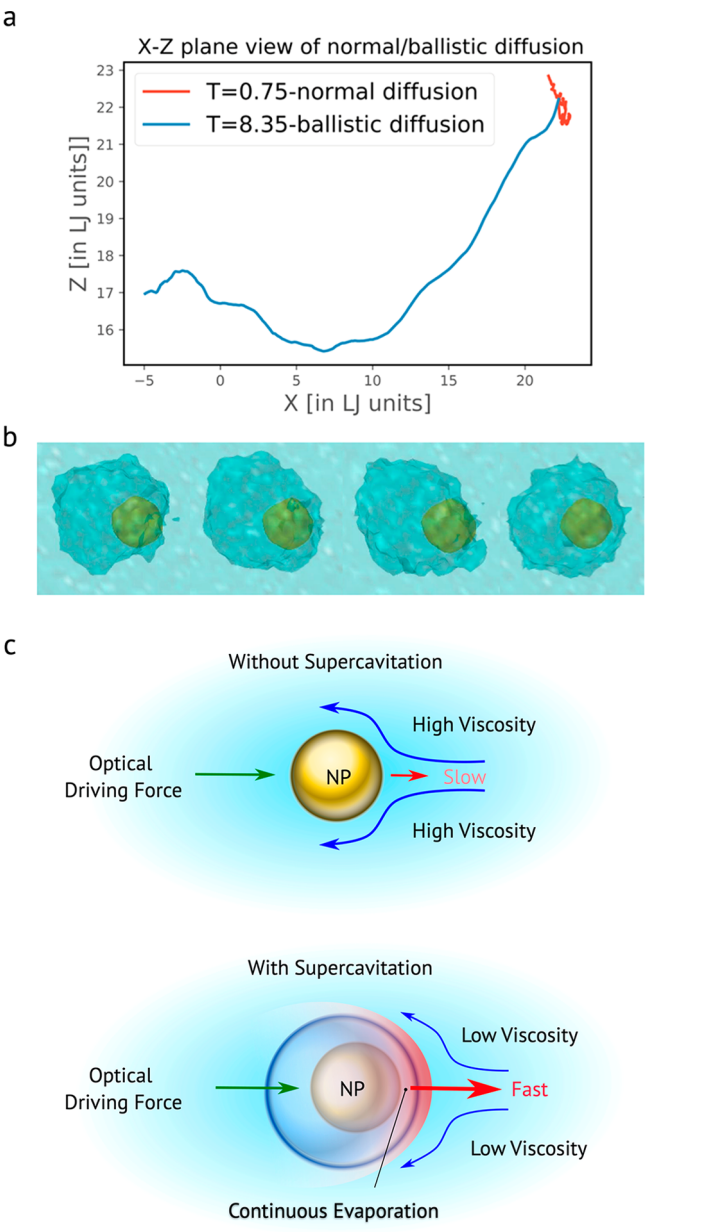

Figure 3. (a) Representative trajectory of the Brownian motion of an NP (T = 0.75 in LJ unit) and a supercavitating NP (T = 8.35 in LJ unit) showing drastically different displacements in the same period of time. (b) MD simulation snapshots of the ballistic Brownian motion of an intensely heated supercavitating NP where the nanobubble boundary is extended as the NP moves due to Leidenfrost effect. (c) Schematic of light-driven NP with and without supercavitation.

https://doi.org/10.1021/acs.jpcc.1c07244
J. Phys. Chem. C XXXX, XXX, XXX−XXX

kept hot in the nanobubble so that it can instantaneously evaporate water as it moves to keep itself in a gaseous environment—a nanoscale analogy of the Leidenfrost effect (Figure 3b). With regard to the accurate modeling of the motion of a supercavitating NP, due to the low viscosity, if a Langevin approach to the driven Brownian motion is used, it would be essential to retain the inertial terms in the Langevin equations to capture the particle dynamics.[43] The experimental observation of such a ballistic Brownian motion of supercavitating NPs has not been made due to the difficulty of keeping the NP hot while applying no additional interference to the dynamics due to factors like optical forces.

A plasmonic heating by a pulsed laser can keep an NP hot to maintain the supercavitating state. After a pulse, the supercavitating NP cools down due to the heat diffusion to the surroundings, and then the nanobubble shrinks and eventually disappears. The nanobubble lifetime is 1−100 ns,[16] but if a subsequent pulse arrives within the lifetime of the nanobubble, the Au NP can be heated again to prevent the nanobubble from collapsing. A pulsed laser with a repetition rate greater than 10 MHz can potentially realize such a situation to keep the supercavitating NP for an extended period of time. In the meantime, the laser also applies optical pressure, which acts as a driving force for the NP to move. The NP is kept hot due to laser irradiation and can instantaneously evaporate water to extend the nanobubble boundary, as it is driven by the laser to move. Lee et al.[10] used a dark-field optical microscope combined with highspeed videography (>5000 frames per second) to investigate the motion of optically driven supercavitating NPs. They also estimated the optical force on the NP with the time-averaged Maxwell's stress tensor based on the electromagnetic field profile obtained using a finite element method or an analytical method with vector spherical harmonics.[44] They observed that the supercavitating NP could move a long distance of 0.1 mm with speed (0.1 m/s) that is almost 100 times faster than a bare NP in water if driven by the same optical force (Figure 3c). Interestingly, Lee et al.[44] also found that, at certain NP-nanobubble geometrical configurations, the photon stream reflected by the water/bubble interface can result in a net optical force on an NP opposite to the light propagation direction. They also observed the superfast backward motion of NPs in the experiment.[10] The supercavitating NP is a thermally nonequilibrium state where continuous photothermal energy conversion, heat transfer, water evaporation, and condensation coexist in the nanoscale. The above picture is based on plausible physical reasoning, and direct experimental observation can be challenging. Fu et al.[29] used a 4D transmission electron microscope (TEM) to directly visualize the NP motion with a plasmonic laser excitation. They found that plasmonic nanobubbles can attach to the surface of NPs and propel them to move. Because of the random orientation of the nanobubble and NP, they observed a forced Brownian motion (i.e., an active Brownian motion) with an instantaneous speed up to ∼6 m/s. It is noted that this active Brownian NP movement at the nanoscale is fundamentally different from the light-driven ballistic supercavitating NP movement, which is driven by an optical force and always aligns with the light axis during the ∼100 μm travel distance.

2.4. Theoretical Modeling. A wide array of theoretical and simulation approaches has been applied to the study of bubble nucleation and dynamics, ranging from continuum theories of varying complexity[18,19,24,38,40,45] to MD simulations.[10,22,37,38,46,47] The classical Rayleigh-Plesset equation has been used to model the bubble dynamics and collapse.[18,40,45] This approach is very successful in modeling the bubble dynamics following a nucleation of the vapor phase. For example, Wang et al.[45] and Zaytsev et al.[40] used complementary experiments and calculations based on the Rayleigh-Plesset equation to find that dissolved gas in the fluid has a profound effect on the bubble collapse dynamics at long times and that the history of bubble dynamics can influence gas adsorption at the liquid−vapor interface. On the one hand, such approaches are very effective in understanding the bubble dynamics, but they do not account for a phase change or the role of NP-fluid thermodynamics. On the other hand, theoretical studies using constitutive models within a phase-field like (so-called dynamic van der Waals) approach[19,24] can successfully capture the phase change and subsequent bubble dynamics in good agreement with the Rayleigh-Plesset description at intermediate-to-long times. Moreover, these models can readily include multiphysics phenomena including NP thermodynamics[19] and solid−fluid interactions.[24] The main advantage to both constitutive hydrodynamic models and the Rayleigh-Plesset equation is that the continuum description can be applied to NPs of arbitrary size for long times at essentially no increase in computational cost for larger NPs. Additionally, the continuum description offers a relatively intuitive understanding of the underlying physics. However, these phase-field/dynamic van der Waals hydrodynamic approaches have relied on simplified fluid models for a single species of molecule and largely ignored the role of dissolved gas and other solutes, which would necessitate the introduction of multiple gradient-density coupling constants into the theory.

Besides constitutive models, MD simulations have been a useful tool for exploring the fundamental physics related to plasmonic nanobubbles, as they can faithfully capture all relevant physics associated with nanobubbles within the simulated model. Many of the above-discussed physics were studied using MD simulations. For example, Sasikumar et al.[22,38] conducted MD simulations to study the cavitation dynamics around intensely heated solid NPs immersed in a model Lennard-Jones (LJ) fluid and observed four stages of bubble asymmetric temporal evolution, providing a detailed understanding of the thermal characteristics during the formation and collapse. MD simulations have also shed light on nanobubble dynamics in a multicomponent fluid. Maheshwari et al.[46] studied the formation of a nanobubble around a heated NP in a model liquid with different concentrations of dissolved gas using MD simulations. They found that, beyond a certain threshold concentration, the dissolved gas dramatically facilitated vapor bubble nucleation due to the formation of gaseous weak spots in the liquid surrounding the NP. MD simulations also provide convenience for parametric studies. For example, Pu et al.[47] found that nanobubbles around heated NPs are generated faster if the NP surface is super-hydrophobic rather than hydrophilic. MD has also helped to understand the ballistic movements of supercavitating NPs and revealed the nanoscale Leidenfrost effect.[10,37]

Ideally, MD can include all the complex factors in realistic nanobubble dynamics around heated NPs, if the force field used in such simulations is accurate and simulation sizes are computationally affordable. However, this is a big "if", since simulating real NPs of tens of nanometers in size in addition to a sizable solvent box can be extremely computationally

https://doi.org/10.1021/acs.jpcc.1c07244
J. Phys. Chem. C XXXX, XXX, XXX−XXX

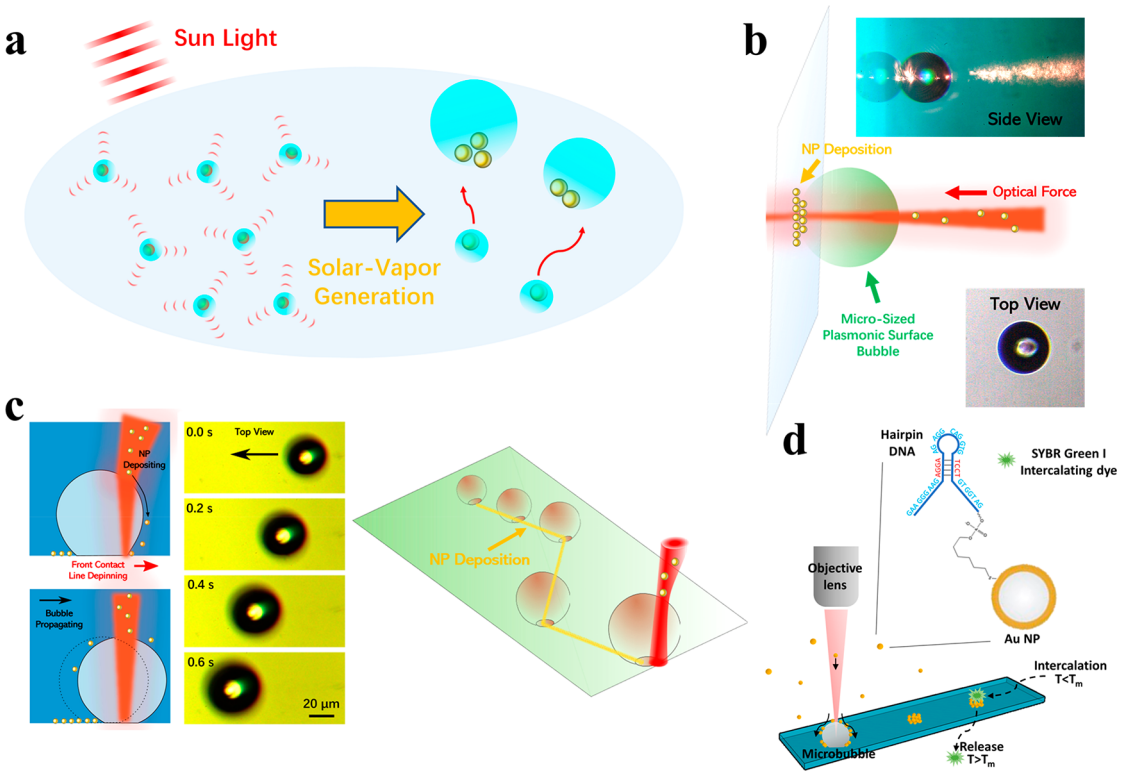

Figure 4. (a) Schematic of the originally believed NP-enabled solar steam generation.[6] (b) Schematic and optical images of the plasmonic surface bubble generated by the optically deposited Au NPs. (c) The schematic and optical images showing the optically directed surface bubble movement and NP deposition process on transparent surfaces. (d) Schematics of the hairpin DNA-functionalized Au NPs deposition and concentration by leveraging the shrinking phase of surface plasmonic bubble.

expensive, not to mention the uncertainty related to force fields for the solvent and between NP and solvent. For example, a simulation of a gold NP immersed in water found no bubble formation even if the NP was heated to ∼900 K,[48] but simulations of model systems of heated solid NPs in argon showed a robust nanobubble formation.[22,37] MD simulations may also be an integral part of multiscale models by providing important input parameters (e.g., interfacial energy, thermal boundary conductance) or thermodynamics equation of state to mesoscale models, but such a promise is still to be filled. It is also desirable that large-scale molecular simulations of a realistic water nanobubble around an NP are more commonly performed instead of just toy models. One promising route to addressing all these issues is the incorporation of machine learning methods, which has already been successfully applied to the study of multiscale cavitation in bulk fluid.[49]

2.5. Applications of Nanobubbles. In the last few decades, the plasmonic nanobubble has been investigated mainly for biomedical applications, such as cell-level therapy[3,50−52] and imaging,[3,50,53−56] controlled drug release and delivery,[1,3,50,57] and microtissue surgery.[3,50,58] The plasmonic photothermal imaging is based on the local variation of refractive index induced by a vapor nanobubble. For instance, Lukianova-Helb et al.[54] could selectively insert core−shell Au NPs with an SPR wavelength of 760 nm in target cells (leukemia cells, lung, and squamous carcinoma cancer cells), and they have confirmed that the NPs form small clusters in the cells. When a pulsed laser tuned at the SPR peak wavelength illuminated these NP clusters, plasmonic nanobubbles were formed. They used these plasmonic nanobubbles as optical amplifiers that increase the scattered intensity of probe light (532 nm) by up to 1800 times compared to that with bare NPs without bubbles. The plasmonic nanobubbles were believed to be an effective way for cell-level imaging without detectable damage to host cells if the laser excitation energy is properly controlled. With a stronger excitation, the expansion of plasmonic nanobubbles can also induce a mechanical shock that can open up the cellular membrane or open an injected liposome to release a drug. These processes can kill target cancer cells[2,59] or achieve intracellular drug delivery and release.[1]

In biomedical applications, the excitation laser should have a frequency in the biological transparent window (650−1350 nm).[60] While solid Au NPs have been a good model system for understanding fundamental physics, their excitation peak would be in the wavelength range where biological tissues are not transparent. Such practical constraints have promoted the design of NPs with suitable SPR frequencies while minimizing the fluence threshold for nanobubble generation. At the near-infrared wavelength of ∼800 nm, which is transparent to most biological tissues, Lachaine et al.[30] have proposed a design rule of silica-core-Au-shell (core−shell (CS)) NP to consider the plasmonic nanobubble threshold fluence and irreversible cell damage. They have found that an optimal CS NP (42 nm silica core and 29 nm Au shell) can have a threshold fluence of 350 J m^{2-} with an off-SPR excitation (pink upward triangle in Figure 1b), where 80% of the CS NPs will not be damaged by overheating after nanobubbles are formed. They have also found that the suboptimal CS NP (cyan pentagram in Figure 1b), which is easy to be damaged due to heating, can have a much lower threshold fluence of 70 J m^{2-}. It is noted that this threshold

https://doi.org/10.1021/acs.jpcc.1c07244
J. Phys. Chem. C XXXX, XXX, XXX−XXX

Table 1. Active Biosensing Applications That Use Plasmonic Surface Bubbles

plasmonic bubble generation	laser wavelength (power density)	bubble size (shrinking/ concentrating time)	strategy for concentrating analytes	target	detection method	LOD
Functionalized Au nanoparticle suspension[5]	800 nm (0.88 mW/μm^2)	~40 μm (~7 min)	Shrinking bubble deposition	Hairpin DNA-functionalized Au NPs	Fluorescence	
3D nanoantennas[68]	850 nm (390 mW/μm^2)	~100 μm (~2 min)	Shrinking bubble deposition	Extracellular membrane vesicles (Evs)	Surface enhanced Raman spectroscopy (SERS)	
Array of Au nanoislands/ Perfluoropentane (PFP)[74]	532 nm (0.26 mW/μm^2)	~20 μm (1 min)	Contact line deposition	FITC-Protein A/G	Fluorescence	10 nM
Moiré Chiral Metamaterials[75]	532 nm (−)	~5 μm (20 min)	Successive microbubble shrinking deposition	Glucose	Circular dichroism	100 pM
Au nanoisland film[69]	785 nm (0.2 mW/μm^2)	~100 μm (ca. tens of min)	Shrinking bubble deposition	4-MBA/R6G	SERS	1 pM/ 100 nM
Accumulation of Au nanoparticles[70] (Nanosphere/ Nanoshell)	1064 nm (10 mW/μm^2)	~175 μm (2 min)	Contact line deposition	R6G/Malachite Green fungicide	SERS (785 nm)	10 fM

fluence is much lower than the predicted value of 200 J m^{2-}, but such a difference was not explained. Ogunyankin et al.[28] have proposed hollow Au shell NPs, achieving a threshold fluence of 20 J m^{2-} with a diameter of 30 nm (gold pentagram in Figure 1b, τ = 28 ps, λ = 800 nm: SPR). Notably, even though they used a picosecond pulsed layer, the recorded threshold fluence is very close to Metwally's prediction with a femtosecond pulsed laser. The nanobubble formation, however, can severely damage the hollow shell Au NP, melting it into a solid sphere.

Plasmonic nanobubbles have also been explored for vapor generation[6,7,61,62] and plasmon-assisted photocatalytic reactions.[8] Neumann et al.[6] dispersed core−shell NPs in water, and when this was irradiated by sunlight, it was believed that the temperature around the NPs was sufficiently high to enable a local vapor formation (i.e., nanobubble). They believe these vapor nanobubbles will coalesce with each other under a continued illumination leading to a larger vapor bubble, which can float toward the water−air interface and then release the vapor (Figure 4a). However, it was later concluded that a nanobubble formation was impossible given the low solar intensity,[61] and the observed water evaporation would be evaporation at the water−air interface. A similar strategy was employed for plasmon-assisted photocatalytic reactions. Adleman et al.[8] used plasmonic NPs as a heterogeneous catalyst to provide both heat and vaporized reactants to the system without excessively heating the immediate surroundings or the preheating needed to vaporize the reactants.

As previously mentioned, the supercavitating NPs can be driven by light. Using this feature, Zhang et al.[63] used light to deposit Au NPs onto the transparent surface by optical forces. The deposited Au NPs become the surface heater triggering the nucleation of a microsized plasmonic surface bubble (Figure 4b).[63,64] The deposited NPs, when heated by a laser, can also help to depin the front contact line of the plasmonic surface bubble, enabling light to guide the surface bubble to move (Figure 4c left panel).[11] As the surface bubble moves with the light, NPs can be deposited along the moving path. This contact-line deposition can be used as a controllable technique for pattern writing (Figure 4c right panel).[12,65] The formed plasmonic surface bubble has also been leveraged for biosensing. The Marangoni flow around the surface bubble helps to bring analytes in the solution to the bubble surface,[66,67] which then deposits the analytes to the contact line of the surface bubble. Leveraging the shrinking phase of the bubble, Moon et al.[5] deposited and concentrated hairpin DNA-functionalized Au NPs on a substrate, which significantly reduced the detection limit by using fluorescence signals (Figure 4d).

Biosensing applications using plasmonic bubbles are still developing, but most such applications leverage the flow surrounding the plasmonic surface bubble. This flow has been called a "bubble tweezer" and can be mainly induced by the difference of bubble/liquid interfacial tension (i.e., Marangoni flow), which depends on temperature gradients. These different biosensing applications leverage similar strategies in generating the surface bubble, where they use the photothermal conversion process occurring in three-dimensional (3D) patterns,[68] optically resistive thin films,[69] or metallic NPs.[5,70] On the one hand, the bubble tweezer can actively capture analytes in the solution and bring them to the three-phase contact lines of the surface bubble. The deposited analytes are later detected via techniques like surface-enhanced Raman spectroscopy (SERS) or fluorescence. On the other hand, using the bubble tweezer can cause the deposited analytes to have a higher temperature, which may deteriorate the function of the analytes. Moon et al.[5] have shown that such heating problems can be avoided when leveraging the shrinkage of the surface bubble after the laser excitation is turned off. In the bubble-shrinking process, the analytes trapped at the surface bubble are eventually deposited at the contact lines without heating. We summarized the studies in biosensing applications in Table 1, which shows that the limit of detection (LOD) can be as low as 10 fM. The LOD is found to inversely correlate with the bubble size.[5] It suggests that larger bubbles would be preferred to lower the LOD. However, it may worsen the damage of analytes by the photothermal heating effect or pose a longer shrinkage time (~hours) when we use the shrinkage bubble.[5] Thus, further research is needed to continue to decrease the LOD so that the bubble-assisted active sensing technology can be used for biomarker detections such as influenza and cancer, which require an LOD in the femto- or atto-molar level.[71−73]

3. CONCLUSION

In this Perspective, we have reviewed the current state of the understanding of the nanobubble formation and dynamics physics, the theoretical modeling effort to describe the multiscale, multiphysics phenomena, and the applications. The minimal threshold fluence for nanobubble formation has

https://doi.org/10.1021/acs.jpcc.1c07244
J. Phys. Chem. C XXXX, XXX, XXX−XXX

been qualitatively described by heat transfer models, but factors like the nature of laser excitation (interband vs SPR) and temperature-dependent optical absorption efficiency need to be considered to improve the model so that their prediction can be closer to experimental data. For more detailed theoretical models, while they have been able to explain important physics underlying the fluence threshold such as NP thermodynamics, interfacial thermal conductance, and dissipation versus phase change, a more accurate thermodynamics equation of the fluid surrounding the intensely heated NP and the treatment of a multicomponent fluid (e.g., dissolved air in water) are the next steps to enhance the capability of these models. MD simulations have been an important tool to provide a molecular-level understanding of nanobubbles, but most of them are of toy models, as they are limited by the computational length and time scales needed to simulate more realistic systems. It is also noted that, currently, no MD simulation has been able to simulate the nanobubble formation of an NP immersed in water, even if the NP is in the system size that a current computation can handle. It is desired that MD simulations can provide key information (e.g., interfacial thermal conductance, equation of state) for mesoscale constitutive models to achieve a more accurate description of nanobubble formation and dynamics. Plasmonic nanobubbles have also seen a number of potential applications; most of them are biomedical-related like cell-level therapy and imaging, controlled drug release and delivery, and microtissue surgery. For these applications, it is important that the energy of the excitation laser can be minimized so as to reduce side effects from the photothermal effect, and thus we have seen an effort to design NPs that can lower the fluence threshold for a plasmonic nanobubble formation. An NP deposited on a surface can lead to plasmonic surface bubbles, which also have wide active biosensing applications, but further research is needed to lower the sensing LOD so that they can be used to practice more challenging detections like those of influenza and cancer.

Overall, a plasmonic nanobubble is a phenomenon that involves complicated and intertwined optical, thermal, and fluidic physics, which needs a multidisciplinary effort to fully understand. New multiscale simulation models need to be developed to accurately describe this phenomenon, but there are challenges to include all the complicated physics into one model. Most of the experimental understandings are based on inferences from microscopic observations. Experimental tools that resolve the time and spatial scales of nanobubbles are needed to better validate modeling results, and high-speed TEM has emerged as a promising tool. Applications may benefit from such fundamental understandings in aspects like optimizing the laser excitation conditions and NP designs.

AUTHOR INFORMATION

Corresponding Authors

Jarrod Schiffbauer − *Department of Physical and Environmental Sciences, Colorado Mesa University, Grand Junction 81501-3122 Colorado, United States*; Email: jschiffbauer@coloradomesa.edu

Eungkyu Lee − *Department of Electronic Engineering, Kyung Hee University, Yongin-si 17104, South Korea*; orcid.org/0000-0002-0211-0727; Email: eleest@khu.ac.kr

Tengfei Luo − *Department of Aerospace and Mechanical Engineering, University of Notre Dame, Notre Dame 46556 Indiana, United States; Department of Chemical and Biomolecular Engineering, University of Notre Dame, Notre Dame 46556 Indiana, United States*; orcid.org/0000-0003-3940-8786; Email: tluo@nd.edu

Authors

Seunghyun Moon − *Department of Aerospace and Mechanical Engineering, University of Notre Dame, Notre Dame 46556 Indiana, United States*; orcid.org/0000-0002-4318-1572

Qiushi Zhang − *Department of Aerospace and Mechanical Engineering, University of Notre Dame, Notre Dame 46556 Indiana, United States*; orcid.org/0000-0003-1313-7965

Zhihao Xu − *Department of Aerospace and Mechanical Engineering, University of Notre Dame, Notre Dame 46556 Indiana, United States*; orcid.org/0000-0003-1054-3669

Dezhao Huang − *Department of Aerospace and Mechanical Engineering, University of Notre Dame, Notre Dame 46556 Indiana, United States*; orcid.org/0000-0002-1413-5438

Seongmin Kim − *Department of Aerospace and Mechanical Engineering, University of Notre Dame, Notre Dame 46556 Indiana, United States*

Complete contact information is available at: https://pubs.acs.org/10.1021/acs.jpcc.1c07244

Notes

The authors declare no competing financial interest.

Biographies

Seunghyun Moon received his Ph.D. degree from the Department of Nano Science and Technology at Seoul National University, South Korea. He joined the University of Notre Dame as a postdoctoral associate in 2019. His research is in 3D printing, micro/nano-fabrications, and biosensors.

Qiushi Zhang completed his Bachelor of Science and M.Phil. degrees in Physics at Hong Kong Baptist University and Hong Kong University of Science and Technology, respectively. He joined the University of Notre Dame in 2018 as a Ph.D. student in the Aerospace and Mechanical Engineering Department. His research interests include bubble dynamics, plasmonic nanoparticles, opto-thermofluids, and their applications.

Zhihao Xu received his bachelor's degree from Xi 'an Jiaotong University in 2020 and later joined the University of Notre Dame to pursue his Ph.D degree. His research interests include multiscale heat transfer and molecular dynamics simulations.

Dezhao Huang completed his Ph.D. in Aerospace and Mechanical Engineering at the University of Notre Dame in 2021 May. He is currently a key postdoctoral fellow at Wuhan University. His research mainly focuses on thermal and mass transport at the solid−liquid material interface.

Seongmin Kim received his Ph.D. in Mechanical Engineering at Pohang University of Science and Technology in 2021. He is currently a postdoctoral researcher in the Aerospace and Mechanical Engineering Department at the University of Notre Dame. His research interests include the fabrication of micro/nanostructured functional materials, development of a design platform for nano materials using machine learning and quantum computing, and their applications.

Jarrod Schiffbauer completed his Ph.D. in Physics at West Virginia University. After postdoctoral research at Technion and University of Notre Dame, he joined Colorado Mesa University in the Department of Physical and Environmental Sciences in 2017, where he is currently a Research Assistant Professor. His research interests span a number

https://doi.org/10.1021/acs.jpcc.1c07244
J. Phys. Chem. C XXXX, XXX, XXX−XXX

of phenomena in nonequilibrium thermodynamics, soft condensed matter, and applications.

Eungkyu Lee received his Ph.D. in Engineering with Nano Science and Technology at Seoul National University. Then, he experienced postdoctoral courses at the University of Notre Dame and joined Kyung Hee University (KHU) in 2021. He is currently an Assistant Professor in the Department of Electronic Engineering at KHU. The research interests cover various topics of energy-and-photonics engineering ranging from fundamental light−matter interactions, nanoscale energy transport and conversion, and their applications.

Tengfei Luo completed his Ph.D. in Mechanical Engineering at Michigan State University. After postdoctoral research at MIT, he joined the University of Notre Dame in 2012, where he is currently a Professor in the Aerospace and Mechanical Engineering Department. His research interests span a broad spectrum in multiscale thermal transport, opto-thermofluids, and their applications.

■ ACKNOWLEDGMENTS

The authors are thankful for the support from multiple National Science Foundation grants (1706039, 1931850, 2040565, and 2001079) and the Center for the Advancement of Science in Space (GA-2018-268). E.L. is also thankful for the support from the National Research Foundation of Korea (NRF) grant funded by the Korea Government (MSIT) (No. NRF-2021R1C1C1006251).

■ REFERENCES

(1) Ghosh, P.; Han, G.; De, M.; Kim, C. K.; Rotello, V. M. Gold nanoparticles in delivery applications. *Adv. Drug Delivery Rev.* **2008**, *60*, 1307−1315.

(2) Lal, S.; Clare, S. E.; Halas, N. J. Nanoshell-enabled photothermal cancer therapy: impending clinical impact. *Acc. Chem. Res.* **2008**, *41*, 1842−1851.

(3) Baffou, G.; Quidant, R. Thermo-plasmonics: using metallic nanostructures as nano-sources of heat. *Laser, Photonics Reviews* **2013**, *7*, 171−187.

(4) Qin, Z.; Bischof, J. C. Thermophysical and biological responses of gold nanoparticle laser heating. *Chem. Soc. Rev.* **2012**, *41*, 1191−1217.

(5) Moon, S.; Zhang, Q.; Huang, D.; Senapati, S.; Chang, H.; Lee, E.; Luo, T. Biocompatible Direct Deposition of Functionalized Nanoparticles using Shrinking Surface Plasmonic Bubble. *Adv. Mater. Interfaces* **2020**, *7*, 2000597.

(6) Neumann, O.; Urban, A. S.; Day, J.; Lal, S.; Nordlander, P.; Halas, N. J. Solar Vapor Generation Enabled by Nanoparticles. *ACS Nano* **2013**, *7*, 42−49.

(7) Pang, Y.; Zhang, J.; Ma, R.; Qu, Z.; Lee, E.; Luo, T. Solar−Thermal Water Evaporation: A Review. *ACS Energy Lett.* **2020**, *5*, 437−456.

(8) Adleman, J. R.; Boyd, D. A.; Goodwin, D. G.; Psaltis, D. Heterogenous catalysis mediated by plasmon heating. *Nano Lett.* **2009**, *9*, 4417−4423.

(9) Liu, G. L.; Kim, J.; Lu, Y.; Lee, L. P. Optofluidic control using photothermal nanoparticles. *Nat. Mater.* **2006**, *5*, 27−32.

(10) Lee, E.; Huang, D.; Luo, T. Ballistic supercavitating nanoparticles driven by single Gaussian beam optical pushing and pulling forces. *Nat. Commun.* **2020**, 48525−48532, DOI: 10.1038/s41467-020-16267-9.

(11) Zhang, Q.; Pang, Y.; Schiffbauer, J.; Jemcov, A.; Chang, H.; Lee, E.; Luo, T. Light-guided surface plasmonic bubble movement via contact line de-pinning by in-situ deposited plasmonic nanoparticle heating. *ACS Appl. Mater. Interfaces* **2019**, *11*, 48525−48532, DOI: 10.1021/acsami.9b16067.

(12) Lin, L.; Peng, X.; Mao, Z.; Li, W.; Yogeesh, M. N.; Rajeeva, B. B.; Perillo, E. P.; Dunn, A. K.; Akinwande, D.; Zheng, Y. Bubble-pen lithography. *Nano Lett.* **2016**, *16*, 701−708.

(13) Lukianova-Hleb, E.; Hu, Y.; Latterini, L.; Tarpani, L.; Lee, S.; Drezek, R. A.; Hafner, J. H.; Lapotko, D. O. Plasmonic nanobubbles as transient vapor nanobubbles generated around plasmonic nanoparticles. *ACS Nano* **2010**, *4*, 2109−2123.

(14) Siems, A.; Weber, S. A.; Boneberg, J.; Plech, A. Thermodynamics of nanosecond nanobubble formation at laser-excited metal nanoparticles. *New J. Phys.* **2011**, *13*, 043018.

(15) Katayama, T.; Setoura, K.; Werner, D.; Miyasaka, H.; Hashimoto, S. Picosecond-to-nanosecond dynamics of plasmonic nanobubbles from pump−probe spectral measurements of aqueous colloidal gold nanoparticles. *Langmuir* **2014**, *30*, 9504−9513.

(16) Lukianova-Hleb, E. Y.; Volkov, A. N.; Lapotko, D. O. Laser pulse duration is critical for the generation of plasmonic nanobubbles. *Langmuir* **2014**, *30*, 7425−7434.

(17) Hashimoto, S.; Werner, D.; Uwada, T. Studies on the interaction of pulsed lasers with plasmonic gold nanoparticles toward light manipulation, heat management, and nanofabrication. *J. Photochem. Photobiol., C* **2012**, *13*, 28−54.

(18) Kotaidis, V.; Plech, A. Cavitation dynamics on the nanoscale. *Appl. Phys. Lett.* **2005**, *87*, 213102.

(19) Lombard, J.; Biben, T.; Merabia, S. Kinetics of Nanobubble Generation Around Overheated Nanoparticles. *Phys. Rev. Lett.* **2014**, *112*, 105701.

(20) Hu, M.; Petrova, H.; Hartland, G. V. Investigation of the properties of gold nanoparticles in aqueous solution at extremely high lattice temperatures. *Chem. Phys. Lett.* **2004**, *391*, 220−225.

(21) Merabia, S.; Keblinski, P.; Joly, L.; Lewis, L. J.; Barrat, J. Critical heat flux around strongly heated nanoparticles. *Phys. Rev. E* **2009**, *79*, 021404.

(22) Sasikumar, K.; Liang, Z.; Cahill, D. G.; Keblinski, P. Curvature induced phase stability of an intensely heated liquid. *J. Chem. Phys.* **2014**, *140*, 234506.

(23) Metwally, K.; Mensah, S.; Baffou, G. Fluence Threshold for Photothermal Bubble Generation Using Plasmonic Nanoparticles. *J. Phys. Chem. C* **2015**, *119*, 28586−28596.

(24) Schiffbauer, J.; Luo, T. Liquid phase stabilization versus bubble formation at a nanoscale curved interface. *Phys. Rev. E: Stat. Phys., Plasmas, Fluids, Relat. Interdiscip. Top.* **2018**, *97*, 033106.

(25) Tascini, A. S.; Armstrong, J.; Chiavazzo, E.; Fasano, M.; Asinari, P.; Bresme, F. Thermal transport across nanoparticle−fluid interfaces: the interplay of interfacial curvature and nanoparticle−fluid interactions. *Phys. Chem. Chem. Phys.* **2017**, *19*, 3244−3253.

(26) Wang, S.; Fu, L.; Zhang, Y.; Wang, J.; Zhang, Z. Quantitative Evaluation and Optimization of Photothermal Bubble Generation around Overheated Nanoparticles Excited by Pulsed Lasers. *J. Phys. Chem. C* **2018**, *122*, 24421−24435.

(27) Fales, A. M.; Vogt, W. C.; Wear, K. A.; Pfefer, J.; Ilev, I. K. Size-dependent thresholds for melting and nanobubble generation using pulsed-laser irradiated gold nanoparticles. *Proceedings SPIE 10509, Plasmonics in Biology and Medicine XV;* SPIE, 2018. DOI: 10.1117/12.2290114

(28) Ogunyankin, M. O.; Shin, J. E.; Lapotko, D. O.; Ferry, V. E.; Zasadzinski, J. A. Optimizing the NIR Fluence Threshold for Nanobubble Generation by Controlled Synthesis of 10−40 nm Hollow Gold Nanoshells. *Adv. Funct. Mater.* **2018**, *28*, 1705272.

(29) Fu, X.; Chen, B.; Tang, J.; Zewail, A. H. Photoinduced nanobubble-driven superfast diffusion of nanoparticles imaged by 4D electron microscopy. *Sci. Adv.* **2017**, *3*, No. e1701160.

(30) Lachaine, R.; Boutopoulos, C.; Lajoie, P.; Boulais, É.; Meunier, M. Rational Design of Plasmonic Nanoparticles for Enhanced Cavitation and Cell Perforation. *Nano Lett.* **2016**, *16*, 3187−3194.

(31) Kreibig, U.; Vollmer, M. In *Optical properties of metal clusters;* Springer Science & Business Media, 2013.

(32) Wilson, O. M.; Hu, X.; Cahill, D. G.; Braun, P. V. Colloidal metal particles as probes of nanoscale thermal transport in fluids. *Phys. Rev. B: Condens. Matter Mater. Phys.* **2002**, *66*, 224301.

https://doi.org/10.1021/acs.jpcc.1c07244
J. Phys. Chem. C XXXX, XXX, XXX−XXX

(33) Ramos-Alvarado, B.; Kumar, S.; Peterson, G. P. Solid−Liquid Thermal Transport and Its Relationship with Wettability and the Interfacial Liquid Structure. *J. Phys. Chem. Lett.* **2016**, *7*, 3497−3501.
(34) Wei, X.; Zhang, T.; Luo, T. Thermal Energy Transport across Hard−Soft Interfaces. *ACS Energy Lett.* **2017**, *2*, 2283−2292.
(35) Evans, R.; Tarazona, P. Theory of Condensation in Narrow Capillaries. *Phys. Rev. Lett.* **1984**, *52*, 557−560.
(36) Binder, K.; Landau, D. P.; Ferrenberg, A. M. Character of the Phase Transition in Thin Ising Films with Competing Walls. *Phys. Rev. Lett.* **1995**, *74*, 298−301.
(37) Huang, D.; Schiffbauer, J.; Lee, E.; Luo, T. Ballistic Brownian motion of supercavitating nanoparticles. *Phys. Rev. E: Stat. Phys., Plasmas, Fluids, Relat. Interdiscip. Top.* **2021**, *103*, 042104.
(38) Sasikumar, K.; Keblinski, P. Molecular dynamics investigation of nanoscale cavitation dynamics. *J. Chem. Phys.* **2014**, *141*, 234508.
(39) Sabzeghabae, A. N.; Devia-Cruz, L. F.; Gutierrez-Herrera, E.; Camacho-Lopez, S.; Aguilar, G. Bubble dynamics of laser-induced cavitation in plasmonic gold nanorod solutions and the relative effect of surface tension and viscosity. *Opt. Laser Technol.* **2021**, *134*, 106621.
(40) Zaytsev, M. E.; Wang, Y.; Zhang, Y.; Lajoinie, G.; Zhang, X.; Prosperetti, A.; Zandvliet, H. J.; Lohse, D. Gas−Vapor Interplay in Plasmonic Bubble Shrinkage. *J. Phys. Chem. C* **2020**, *124*, 5861−5869.
(41) Manoharan, V. N. Molecular Forces and Self Assembly: In Colloid, Nano Sciences and Biology. *Phys. Today* **2011**, *64*, 48−48.
(42) Rings, D.; Schachoff, R.; Selmke, M.; Cichos, F.; Kroy, K. Hot brownian motion. *Phys. Rev. Lett.* **2010**, *105*, 090604.
(43) Coffey, W.; Kalmykov, Y. P. In *The Langevin equation: with applications to stochastic problems in physics, chemistry and electrical engineering;* World Scientific, 2012.
(44) Lee, E.; Luo, T. Long-distance optical pulling of nanoparticle in a low index cavity using a single plane wave. *Science Advances 6* (**2020**). DOI: 10.1126/sciadv.aaz3646
(45) Wang, Y.; Zaytsev, M. E.; The, H. L.; Eijkel, J. C.; Zandvliet, H. J.; Zhang, X.; Lohse, D. Vapor and gas-bubble growth dynamics around laser-irradiated, water-immersed plasmonic nanoparticles. *ACS Nano* **2017**, *11*, 2045−2051.
(46) Maheshwari, S.; van der Hoef, M.; Prosperetti, A.; Lohse, D. Dynamics of Formation of a Vapor Nanobubble Around a Heated Nanoparticle. *J. Phys. Chem. C* **2018**, *122*, 20571−20580.
(47) Pu, J. H.; Sun, J.; Wang, W.; Wang, H. S. Generation and Evolution of Nanobubbles on Heated Nanoparticles: A Molecular Dynamics Study. *Langmuir* **2020**, *36*, 2375−2382.
(48) Chen, X.; Munjiza, A.; Zhang, K.; Wen, D. Molecular dynamics simulation of heat transfer from a gold nanoparticle to a water pool. *J. Phys. Chem. C* **2014**, *118*, 1285−1293.
(49) Lin, C.; Li, Z.; Lu, L.; Cai, S.; Maxey, M.; Karniadakis, G. E. Operator learning for predicting multiscale bubble growth dynamics. *J. Chem. Phys.* **2021**, *154*, 104118.
(50) Lapotko, D. Plasmonic nanoparticle-generated photothermal bubbles and their biomedical applications. *Nanomedicine* **2009**, *4*, 813.
(51) Lukianova-Hleb, E.; Hanna, E.; Hafner, J.; Lapotko, D. Tunable plasmonic nanobubbles for cell theranostics. *Nanotechnology* **2010**, *21*, 085102.
(52) Hirsch, L. R.; Stafford, R. J.; Bankson, J. A.; Sershen, S. R.; Rivera, B.; Price, R. E.; Hazle, J. D.; Halas, N. J.; West, J. L. Nanoshell-mediated near-infrared thermal therapy of tumors under magnetic resonance guidance. *Proc. Natl. Acad. Sci. U. S. A.* **2003**, *100*, 13549−13554.
(53) Lukianova-Hleb, E.; Kim, Y.; Belatsarkouski, I.; Gillenwater, A. M.; O'Neill, B. E.; Lapotko, D. O. Intraoperative diagnostics and elimination of residual microtumours with plasmonic nanobubbles. *Nat. Nanotechnol.* **2016**, *11*, 525−532.
(54) Hleb, E. Y.; Hu, Y.; Drezek, R. A.; Hafner, J. H.; Lapotko, D. O. Photothermal bubbles as optical scattering probes for imaging living cells. *Nanomedicine* **2008**, *3*. DOI: 10.2217/17435889.3.6.797
(55) Lapotko, D. O.; Lukianova, E. Y. Influence of physiological conditions on laser damage thresholds for blood, heart, and liver cells. *Lasers Surg. Med.* **2005**, *36*, 13−21.
(56) Boyer, D.; Tamarat, P.; Maali, A.; Lounis, B.; Orrit, M. Photothermal imaging of nanometer-sized metal particles among scatterers. *Science* **2002**, *297*, 1160−1163.
(57) Timko, B. P.; Dvir, T.; Kohane, D. S. Remotely triggerable drug delivery systems. *Adv. Mater.* **2010**, *22*, 4925−4943.
(58) Urban, A. S.; Pfeiffer, T.; Fedoruk, M.; Lutich, A. A.; Feldmann, J. Single-step injection of gold nanoparticles through phospholipid membranes. *ACS Nano* **2011**, *5*, 3585−3590.
(59) Stern, J. M.; Stanfield, J.; Kabbani, W.; Hsieh, J.; Cadeddu, J. A. Selective prostate cancer thermal ablation with laser activated gold nanoshells. *J. Urol.* **2008**, *179*, 748−753.
(60) Smith, A. M.; Mancini, M. C.; Nie, S. Second window for in vivo imaging. *Nat. Nanotechnol.* **2009**, *4*, 710−711.
(61) Fang, Z.; Zhen, Y.; Neumann, O.; Polman, A.; de Abajo, F. J. G.; Nordlander, P.; Halas, N. J. Evolution of light-induced vapor generation at a liquid-immersed metallic nanoparticle. *Nano Lett.* **2013**, *13*, 1736−1742.
(62) Dongare, P. D.; Alabastri, A.; Neumann, O.; Nordlander, P.; Halas, N. J. Solar thermal desalination as a nonlinear optical process. *Proc. Natl. Acad. Sci. U. S. A.* **2019**, *116*, 13182−13187.
(63) Zhang, Q.; Li, R.; Lee, E.; Luo, T. Optically Driven Gold Nanoparticles Seed Surface Bubble Nucleation in Plasmonic Suspension. *Nano Lett.* **2021**, *21*, 5485−5492.
(64) Zhang, Q.; Neal, R. D.; Huang, D.; Neretina, S.; Lee, E.; Luo, T. Surface Bubble Growth in Plasmonic Nanoparticle Suspension. *ACS Appl. Mater. Interfaces* **2020**, *12*, 26680−26687.
(65) Fujii, S.; Fukano, R.; Hayami, Y.; Ozawa, H.; Muneyuki, E.; Kitamura, N.; Haga, M. Simultaneous formation and spatial patterning of zno on ito surfaces by local laser-induced generation of microbubbles in aqueous solutions of [Zn (NH3) 4] 2. *ACS Appl. Mater. Interfaces* **2017**, *9*, 8413−8419.
(66) Namura, K.; Nakajima, K.; Kimura, K.; Suzuki, M. Photo-thermally controlled Marangoni flow around a micro bubble. *Appl. Phys. Lett.* **2015**, *106*, 043101.
(67) Namura, K.; Nakajima, K.; Suzuki, M. Quasi-stokeslet induced by thermoplasmonic Marangoni effect around a water vapor microbubble. *Sci. Rep.* **2017**, *7*, 45776.
(68) Tantussi, F.; Messina, G. C.; Capozza, R.; Dipalo, M.; Lovato, L.; De Angelis, F. Long-Range Capture and Delivery of Water-Dispersed Nano-objects by Microbubbles Generated on 3D Plasmonic Surfaces. *ACS Nano* **2018**, *12*, 4116−4122.
(69) Kang, Z.; Chen, J.; Ho, H. Surface-enhanced Raman scattering via entrapment of colloidal plasmonic nanocrystals by laser generated microbubbles on random gold nano-islands. *Nanoscale* **2016**, *8*, 10266−10272.
(70) Karim, F.; Vasquez, E. S.; Sun, Y.; Zhao, C. Optothermal microbubble assisted manufacturing of nanogap-rich structures for active chemical sensing. *Nanoscale* **2019**, *11*, 20589−20597.
(71) Zhang, S.; Garcia-D'Angeli, A.; Brennan, J. P.; Huo, Q. Predicting detection limits of enzyme-linked immunosorbent assay (ELISA) and bioanalytical techniques in general. *Analyst* **2014**, *139*, 439−445.
(72) Munge, B. S.; Coffey, A. L.; Doucette, J. M.; Somba, B. K.; Malhotra, R.; Patel, V.; Gutkind, J. S.; Rusling, J. F. Nanostructured immunosensor for attomolar detection of cancer biomarker interleukin-8 using massively labeled superparamagnetic particles. *Angew. Chem.* **2011**, *123*, 8061−8064.
(73) Wang, Z.; Zhang, J.; Guo, Y.; Wu, X.; Yang, W.; Xu, L.; Chen, J.; Fu, F. A novel electrically magnetic-controllable electrochemical biosensor for the ultra sensitive and specific detection of attomolar level oral cancer-related microRNA. *Biosens. Bioelectron.* **2013**, *45*, 108−113.
(74) Kim, Y.; Ding, H.; Zheng, Y. Enhancing surface capture and sensing of proteins with low-power optothermal bubbles in a biphasic liquid. *Nano Lett.* **2020**, *20*, 7020−7027.
(75) Liu, Y.; Wu, Z.; Kollipara, P. S.; Montellano, R.; Sharma, K.; Zheng, Y. Label-Free Ultrasensitive Detection of Abnormal Chiral Metabolites in Diabetes. *ACS Nano* **2021**, *15*, 6448−6456.

https://doi.org/10.1021/acs.jpcc.1c07244
J. Phys. Chem. C XXXX, XXX, XXX−XXX

(76) Lombard, J.; Biben, T.; Merabia, S. Threshold for Vapor Nanobubble Generation Around Plasmonic Nanoparticles. *J. Phys. Chem. C* **2017**, *121* (28), 15402−15415.

https://doi.org/10.1021/acs.jpcc.1c07244
J. Phys. Chem. C XXXX, XXX, XXX−XXX